J Mater Sci (2007) 42:3670–3674
DOI 10.1007/s10853-006-1348-1

Effect of Li/Nb ratio on structure and photorefractive properties of Zn:Fe:$LiNbO_3$ crystals

X. H. Zhen · Q. Li · L. C. Zhao · Y. H. Xu

Received: 7 February 2005 / Accepted: 27 February 2006 / Published online: 30 January 2007

Abstract Zn:Fe:$LiNbO_3$ crystals with different Li/Nb ratios in the melts (Li/Nb = 0.946, 0.97, 1.00, 1.10, 1.20, 1.44) have been grown for the first time. The UV–Vis absorption spectra, exponential gain coefficient, diffraction efficiency and response time of the crystals were measured. With the ratio of Li/Nb increasing, the absorption edge shifts to a shorter wavelength, the exponential gain coefficient and response speed increase, but the diffraction efficiency decreases.

Introduction

$LiNbO_3$ crystal is one of the most widely used electro-optical materials. Its most important application is holographic storage because of its excellent photorefractive properties. Almost all commercially available $LiNbO_3$ crystals are typical non-stoichiometric compositions, which are grown from a congruent composition melt (Li/Nb = 0.946, atomic ratio) [1]. Although congruent $LiNbO_3$ (labeled CLN) crystals generally have good quality and uniformity, the near stoichiometric $LiNbO_3$ crystals with fewer defects are thought to have superior properties because of higher Li content in crystal lattice. In fact, many $LiNbO_3$ crystal physical properties, such as response time [2], exponential gain coefficient [3], sensitivity and dynamic range [4], electro-ferroelectric [5], absorption edge [6], and optical damage [7], are affected (some with considerable sensitivity) by the Li/Nb ratio in the crystal and by impurities [8, 9].

In this paper, a series of Zn:Fe:$LiNbO_3$ crystals with different Li/Nb ratios were grown. The dependence of photorefractive properties on the Li/Nb ratio is investigated. The UV–Vis absorption spectra were measured to study the structure of the crystals.

Experimental

Sample preparation

Zn:Fe:$LiNbO_3$ crystals were grown along *c* axis from the melt with various Li/Nb ratios in a platinum crucible by the Czochralski method. The starting materials were Li_2CO_3, Nb_2O_5, ZnO and Fe_2O_3 with purity of 99.99%. The melt composition for several crystals is shown in Table 1. In order to prepare the doped $LiNbO_3$ polycrystalline materials, the thoroughly-mixed raw materials were put into a platinum (Pt) crucible (70 mm in diameter and 50 mm in height), and calcined at 750 and 1100 °C for 3 h, respectively. The technical conditions of the crystal growth were listed in Table 1. For the successful growth of good quality crystals a steep thermal gradient above the melt (200–600 °C/cm) was required. To keep the composition homogeneity, the crystal

X. H. Zhen · Q. Li (✉)
Department of Chemistry, Tsinghua University, Beijing 100084, P. R. China
e-mail: qiangli@mail.tsinghua.edu.cn

L. C. Zhao
School of Material Science and Engineering, Harbin Institute of Technology, Harbin 150001, P. R. China

Y. H. Xu
Department of Applied Chemistry, Harbin Institute of Technology, Harbin 150001, P. R. China

Table 1 Growth methods and composition of the Zn:Fe:LN crystals

	No.1	No.2	No.3	No.4	No.5	No.6	No.7	No.8
ZnO (mol %)	0	0	6.0	6.0	6.0	6.0	6.0	6.0
Fe_2O_3 (wt%)	0	0.015	0.015	0.015	0.015	0.015	0.015	0.015
Li/Nb in melt	0.946	0.946	0.946	0.97	1.00	1.10	1.20	1.44
Crystal size (mm^2)	φ 30 × 40	φ 30 × 30	φ 25 × 20	φ 25 × 20	φ 20 × 20	φ 20 × 20	φ 20 × 20	φ 20 × 20
Growth rate (mm/h)	2.0	1.5	1.5	1.0	0.5	0.4	0.2	0.2
Rotation rate(r/min)	12	12	15	15	20	20	20	20
ZnO in crystal (mol %)[a]	0	0	5.38	5.31	4.87	4.69	4.31	3.06
Absorption edge (nm)	323	370	362	361	353	351	346	342

[a] It was measured by X-ray fluorescence analysis

growth was abruptly stopped when about 10 wt.% of the initial charge had pulled out, and slowly cooled down to room temperature at a rate of 100 °C/h. All of the crystals were clear and transparent. Test samples with size of 10 × 10 × 3 mm^3 and 10 × 10 × 1 mm^3, respectively, were cut from the middle of the crystal and polished to optical grade smoothness. The size of the samples is listed in Table 1.

After being eroded by mixed acid (HNO_3:HF = 1:1, volume ratio) at about 100 °C for 0.5 h, the faces of the samples were observed by a metalloscope (XJZ-6, CHINA), many regular triangle pits were found in the face of the as-grown Zn:Fe:$LiNbO_3$ obtained from the melt with the Li/Nb ratio of 1.44. It is confirmed that it was single domain, but other crystals still were multi-domain. After the crystals with multi-domain were polarized in a furnace where the temperature gradient was below 5 °C/cm for polarizing. After being held at a temperature of 1200 °C for 8 h, the crystals were polarized with 5 mA/cm^2 current density. All crystals were cut into wafers for being used in our experiments.

Sample measurements

The UV–Vis optical absorption spectra of the Zn:Fe:$LiNbO_3$ crystals with thickness of 3 mm were measured utilizing a Cary 50 UV–Vis Spectrophotometer of CARY mode. The measurement range was from 300 to 1000 nm, scan speed was 200 nm/s, and data acquisition speed was 80 times/s.

The two-wave coupling experiment was carried out to measure the photorefractive properties of the samples. The experimental setup is shown in Fig. 1. An Ar^+ laser operating at 488.0 nm with the polarizing direction in the incident plane was used as the light source. The diameter of pump light beam and signal light beam was 3 and 1 mm, respectively. The intensity of the pump light beam was 6.50 W/cm^2, and the modulation index of 1830 was selected.

The exponential gain coefficient is one of the important indicators to evaluate the photorefractive properties of crystals, which represents the ability to transit energy from the pump light with high power to signal light. The exponential gain coefficient Γ can be gained by

$$\Gamma = \frac{1}{d}\ln\frac{I_1' I_2}{I_1 I_2'} \quad (1)$$

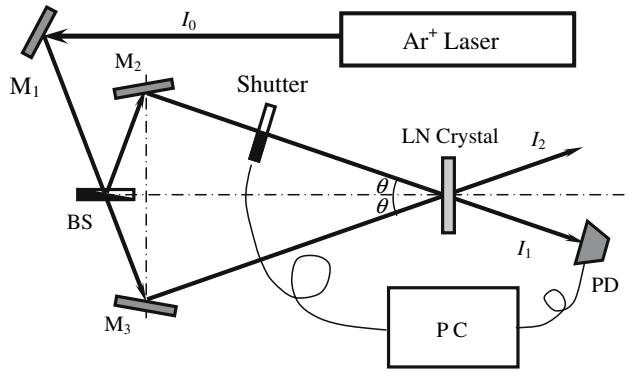

Fig. 1 Experimental setup of two-wave coupling M_1, M_2 and M_3: mirrors; BS: beam splitter; PD: powder detector; I_1 and I_2: T transmitted light of signal light and pump light, respectively

where d is the thickness of the sample, I_1 and I_2 (I_1' and I_2') is the transmitted (diffraction) light intensity of signal beam and pump beam with (without) coupling, respectively. When the intensity of pump beam is much larger than that of signal beam, i.e. $I_2 >> I_1$, the exponential gain coefficient Γ is independent of the intensity of pump light ($I_2 \approx I_2'$).

$$\Gamma = \frac{1}{d}\ln\frac{I_1'}{I_1} \tag{2}$$

The diffraction efficiency is one important parameter for crystal used in holographic storage. The diffraction efficiency η is defined as the ratio of the intensity of the diffracted beam I_2', and the transmitted beam I_2, i.e.

$$\eta = (I_2'/I_2) \times 100\% \tag{3}$$

The response time (τ) is anther important parameter for $LiNbO_3$ crystal. τ is a time period, defined as from the time that the incident light begins to shot on the crystal to the time that diffraction efficiency reaches its maximum.

During erasure of a grating, the photoconduction acts as the main role. At this time, the diffusion field E_{SC} in crystals is

$$E_{SC}(x,t) = E_{SC}(x)e^{-\sigma_{ph}t/\varepsilon} \tag{4}$$

Because the diffraction efficiency $\sqrt{\eta}$ is nearly the direct proportion to the diffusion field E_{SC}, above equation can be changed to by the logarithmic transformation

$$\ln(\eta/\eta_0) = \frac{2\sigma_{ph}}{\varepsilon}t + \text{constant} \tag{5}$$

where η_0 is the maximum of the diffraction efficiency, σ_{ph} is the photoconduction, and ε is the dielectric constant of the material. It can be seen from Eq. (5) that σ_{ph} is the slope rate of the line $\ln(\eta/\eta_0)$~$2t/\varepsilon$ [10].

Results and discussion

Figure 2 shows the UV–Vis absorption spectra of the Zn:Fe:$LiNbO_3$ crystals with various Li/Nb ratios. After Földvári found that the position of the fundamental absorption edge is very sensitive to the composition and defect structure of $LiNbO_3$ [11], many scholars started an extensive study of the absorption edge in $LiNbO_3$ crystals [12–15]. But to our knowledge, there

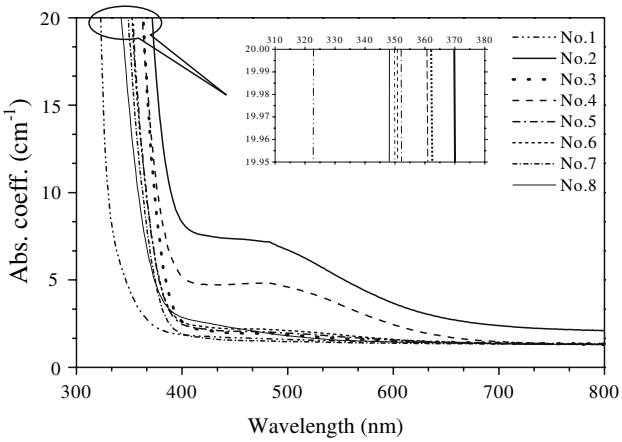

Fig. 2 UV–Vis absorption spectra of the pure congruent $LiNbO_3$, Fe:$LiNbO_3$, and Zn:Fe:$LiNbO_3$ crystals with various Li/Nb ratio and their part magnify figure

is few report [16] about the shift mechanism of the fundamental absorption edge in the UV–Vis absorption spectra of the $LiNbO_3$ crystals until now.

The absorption edge position of different samples can be compared by the wavelength where the absorption coefficient is equal to a certain value. In this work we use optical absorption coefficient α = 20 cm^{-1} as was introduced by Földvári et al. [11, 17]. The absorption edges of the samples were measured and the results were listed in Table 1. In the UV–Vis absorption spectra of the Zn:Fe:$LiNbO_3$ crystals with various Li/Nb ratios (No.3, No.4, No.5, No.6, No.7, and No.8), the absorption edges shift to a shorter wavelength with the Li/Nb ratio in the melts increasing. In $LiNbO_3$ crystal, the relationship between the UV–Vis absorption edge and crystal composition is non-linear, this results is consistent with the former research [18].

According to the previous research [16], it is considered that, in the Zn:Fe:$LiNbO_3$ crystals with high Li/Nb ratio (> 0.946), the number of the Li^+ that connects with O^{2-} is more than that of the No.3 sample. In this paper, the phenomenon of the absorption edge shift is explained by Z^{*2}/r, where $Z^* = Z - \Sigma s$, Z^*, Z, Σs and r are the effective nuclear charge number, the atomic ordinal number of the ion, the shield factor, and the radius of the ion, respectively. The value of Z^* for Li^+ is much lower than that of Nb_{Li}^{4+} and Zn^{2+}, the absorption edges of the Zn:Fe:$LiNbO_3$ crystals (No.4, No.5, No.6, No.7, and No.8) shift to shorter wavelengths compared with that of the No.3 sample, and the shift extent increases with the Li/Nb ratio in the melts increasing.

All the experimental results of two-wave coupling for Zn:Fe:$LiNbO_3$ doped with different Li/Nb ratio $LiNbO_3$ are shown in Table 2. λ is the wavelength

Table 2 Two-wave coupling experimental results of the samples

Sample	λ(nm)	d (mm)	Γ (cm^{-1})	2θ (°)	η(%)	τ(s)
No.1	488.0	0.91	15.3	19.0	27.6	192
No.2	488.0	0.92	21.6	19.0	56.2	163
No.3	488.0	0.91	20.3	19.0	45.8	115
No.4	488.0	0.91	22.0	19.0	37.1	97
No.5	488.0	0.91	23.4	19.0	29.5	81
No.6	488.0	0.90	29.5	19.0	18.4	60
No.7	488.0	0.92	34.7	19.0	9.5	36
No.8	488.0	0.91	37.2	19.0	4.3	17

of the light source, d is the thickness of the samples, 2θ is the included angle between the pump light beam and the signal light beam.

From above mentioned experiments, one can see many regularizing phenomena: The diffraction efficiency (η) of No.1 is lower than that of Fe:$LiNbO_3$ (No.2) and Zn:Fe:$LiNbO_3$ crystals (No.3, No.4, No.5, No.6, No.7, and No.8). In the Zn:Fe:$LiNbO_3$ crystals, the exponential gain coefficient increases, the response time shortens, and the diffraction efficiency decreases with the Li/Nb ratio increasing. According to the well-known scalar expression (Eq. (6)):

$$\Delta n = \frac{Rk\beta I}{\sigma} \tag{6}$$

where Δn is change of refractive index, R is the generalized electro-optical coefficient, k is the Glass constant, β is the optical absorption coefficient, $\sigma = \sigma_d + \sigma_{ph}$ ($\sigma_d << \sigma_{ph}$) σ_d is the dark conductivity, σ_{ph} is the photoconductivity, and I is the light intensity [19, 20]. With an increase of cation-vacancy photoconductivity, the photorefraction decreases because of the increase in photoconductivity, whereas the photovoltaic current is almost unchanged. If an iron impurity is present, an abrupt decrease in the capture cross section of Fe^{3+} acceptors should be responsible for the observed increase in σ_{ph}. Nb_{Li}^{4+} is the most probable electron acceptor in a Li-deficient $LiNbO_3$ host. Thus a reduced Nb_{Li} concentration would lead to an increase of photoconductivity if the concentration of the concurrent Fe^{3+} acceptor is negligible [21]. In $LiNbO_3$ crystal, we may attribute the increase of σ_{ph} to the decrease of the Nb_{Li} concentration due to the site of Nb_{Li} is replaced by the impurities. But in Fe:$LiNbO_3$, because Fe^{3+} substitutes the Li^+, the role of Nb_{Li}^{4+} becomes negligible, and σ_{ph} is governed by the electron acceptor Fe^{3+}. So the Δn of the Fe:$LiNbO_3$ (No.2) is larger than that of the pure $LiNbO_3$ (No.1). According to Eq. (7)) [22]:

$$\eta = \exp(-\beta d/\cos\theta)\sin^2(\pi d\Delta n/\lambda\cos\theta) \tag{7}$$

The η increases with the Δn increasing. In the Zn:Fe:$LiNbO_3$ crystals, the Zn^{2+} substitutes the Nb_{Li}^{4+}, and σ_{ph} rapidly increases because Nb_{Li}^{4+} is vanished and most of the Fe ions substitute Nb^{5+}. With the ratios of Li/Nb ratio increasing, the number of the Fe ions decreases. Therefore, the diffraction efficiency decreases and response time increase due to the photoconduction increasing. The exponential gain coefficient increase owing to the defects (Nb_{Li}^{4+} and Fe ions) decreasing.

Conclusions

In Zn:Fe:$LiNbO_3$ crystals, with the ratio of Li/Nb increasing, the absorption edge shifts to a shorter wavelength, the exponential gain coefficient and response speed increase, but the diffraction efficiency decreases. All these are induced by the intrinsic defects decreasing in the Zn:Fe:$LiNbO_3$ crystals. Zn:Fe:$LiNbO_3$ crystals grown from high Li/Nb melt with good quality are more promising materials used in the holographic storage than congruent Zn:Fe:$LiNbO_3$ crystals.

Acknowledgements This work is sponsored by National Major Project of Fundamental Research of China (G19990330) and China Postdoctoral Science Foundation.

References

1. Wang HL, Hang Y, Zhang LH, Xu J, He MZ, Zhu SN, Zhu YY, Zhou SM (2004) J Cryst Growth 262:313
2. Chen XJ, Zhu DS, Li B, Ling T, Wu ZK (2001) Opt Lett 26:998
3. Chen XJ, Li B, Xu JJ, Zhu DS, Pan SH, Wu ZK (2001) J Appl Phys 90:1516
4. Galambos L, Orlov SS, Hessenlink L, Furukawa Y, Kitamura K, Takekawa S (2001) J Cryst Growth 229:228
5. Abdi F, Aillerie M, Bourson P, Fontana MD, Polgar K (1998) J Appl Phys 84:2251
6. Sun DL, Hang Y, Zhang LH (2002) J Synthetic Cryst 31:314
7. Furukawa Y, Sato M, Kitamura K, Yajima Y, Minakata M (1992) J Appl Phys 72:3250
8. Serrano MD, Bermudez V, Arizmendi L, Didguez E (2000) J Cryst Grow 210:670
9. Bryan DA, Gerson R, Tomaschke HE (1984) Appl Phys Lett 44:847
10. Bienvenu MP, Woodbury D, Robson TA (1980) J Appl Phys 51:4245
11. Földvári I, Polgár K,Voszka R, Balasanyan RN (1984) Cryst Res Technol 19:1659
12. Kovács L, Ruschhaupt G, Polgár K, Corradi G, Wöhlecke M (1997) Appl Phys Lett 70:2801
13. Jin BM, Kim IW, White WB, Bhalla AS (1997) Mater Lett 30:385

14. Liu Y, Kitamura K, Takekawa S, Ravi G, Nakaurua M, Hatano H, Yamaji T (2002) Appl Phys Lett 81:2686
15. Zhang G, Tomita Y, Zhang X, Xu J (2002) Appl Phys Lett 81:1393
16. Zhen XH, Zhao LC, Xu YH (2003) Appl Phys B 76:655
17. Polgár K, Péter Á, Kovács L, Corradi G, Szaller Zs (1997) J Cryst Growth 177:211
18. Wöhleke M, Corradi G, Betzler K (1996) Appl Phys B 63:323
19. Zhang Y, Xu YH, Li MH, Zhao YQ (2001) J Cryst Growth 233:537
20. Volk T, Rubinina N, Wöhlecke M (1994) J Opt Soc Am B 11:1681
21. Donnerberg H, Tomlison SM, Catlow CRA, Schirmer OF (1989) Phys Rev B 40:11909
22. Kogelink H (1969) Bell Syst Tech J 48:2909